Experimental investigation of hydrogen breakthrough pressure for a clay-rich caprock

International Journal of Hydrogen Energy 241 (2026) 155462

Contents lists available at ScienceDirect

International Journal of Hydrogen Energy

journal homepage: www.elsevier.com/locate/he

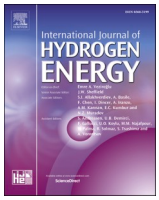

Experimental investigation of hydrogen breakthrough pressure for a clay-rich caprock

Nacer Benlalam [a,*], Nicolò Santi Vasile [a], Costanzo Peter [a], Vera Rocca [a], Dario Viberti [a], Fabrizio Pirri [b,c], Vincenzo Pozzovivo [d], Andrea Mantegazzi [d], Christian Coti [d], Francesca Verga [a]

[a] Politecnico di Torino, Department of Environment, Land and Infrastructure Engineering, Corso Duca degli Abruzzi 24, 10129, Torino, Italy
[b] Politecnico di Torino, Department of Applied Science and Technology, Corso Duca degli Abruzzi 24, 10129, Torino, Italy
[c] Centre for Sustainable Future Technologies, Fondazione Istituto Italiano di Tecnologia, Via Livorno 60, 10144, Torino, Italy
[d] Snam-Stogit, Via Libero Comune, 5, 26013, Crema, Italy

ARTICLE INFO

Keywords:
Threshold pressure
Breakthrough pressure
Caprock
Underground hydrogen storage
Underground energy systems

ABSTRACT

We performed laboratory experiments using customized equipment to measure the breakthrough pressure of hydrogen on plugs retrieved from a clay-rich caprock, named Argille del Santerno Formation. This formation overlies several Italian depleted gas reservoirs currently utilized for natural gas storage but under consideration for conversion into hydrogen storages. After characterizing the caprock (grain size and mineralogy), a set of 9 preserved and fresh plugs was subject to step-by-step tests to measure the breakthrough pressure of hydrogen. To the best of the authors' knowledge, these are the first reported experiments of breakthrough pressure measurements with hydrogen on plugs obtained from a real caprock. The obtained values range from 25 to 80 bars and compare well to previously reported values for nitrogen and methane, measured on the same caprock under the same testing conditions. Results confirm that hydrogen can be safely stored in the depleted gas reservoirs, even under deltapressure conditions.

1. Introduction

Hydrogen is a key enabler of the global energy transition, offering a sustainable pathway to decarbonize energy systems and reduce reliance on fossil fuels, thereby helping to curb global warming [1–3]. As a versatile energy carrier, hydrogen supports the integration of renewable energy by enabling long-term energy storage and addressing the variability of solar and wind power [4]. As hydrogen gains prominence as an energy carrier, the need for large-scale, efficient, and safe storage solutions becomes increasingly critical [1,5], and Underground Hydrogen Storage (UHS) is key to managing supply and demand fluctuations and enabling hydrogen integration into energy grids and industrial applications [3,6,7].

Like natural gas, hydrogen can be stored in geological formations such as salt caverns, depleted oil and gas reservoirs, and aquifers. Advancements in underground hydrogen storage draw heavily on decades of experience with natural gas storage, leveraging established technologies and infrastructure. However, hydrogen properties are unique [8–11], and additional aspects need to be investigated when hydrogen rather than natural gas is injected underground. One of the most significant issues is related to the bio-geochemical reactions. Deep geological formations can host microorganisms (in particular, hydrogenotrophic methanogens, acetogenic bacteria, and sulphate-reducing bacteria) that could cause hydrogen consumption, biocorrosion, and pore-clogging due to biofilm formation and biomass accumulation, formation water acidification, and safety risks due to the production of H_2S. Thus, extensive experimental investigations and modeling studies are undertaken to verify the existence and potential proliferation of microorganisms in porous media when storing hydrogen underground [12–19]. Another critical aspect is the confinement ability of the caprock overlying the reservoir. Typically, caprocks are fine-grained, low-permeability sedimentary formations with poor transport capacity, which is well proven by their ability to retain hydrocarbons over geological timescales [20]. However, hydrogen molecules are smaller than methane molecules (the molecular diameter of H_2 is 0.24 nm, while that of CH_4 is 0.68 nm); thus, concerns about hydrogen diffusion

* Corresponding author.
E-mail address: nacer.benlalam@polito.it (N. Benlalam).

https://doi.org/10.1016/j.ijhydene.2026.155462
Received 27 November 2025; Received in revised form 17 April 2026; Accepted 7 May 2026
Available online 16 May 2026

through the water phase saturating the caprock are also being addressed [21–23]. Additionally, hydrogen is characterized by a volumetric density that is 8 times less than methane [12,24], requiring higher operating pressures to match the same storage capacity and working gas granted by a natural gas storage. If the maximum operating pressure is designed to exceed the original formation pressure (deltapressure conditions), additional investigations are needed to confirm that gas leakage through the caprock would not occur [20,24,25]. Capillary forces are responsible for preventing hydrocarbons from migrating across the caprock due to their buoyancy. The threshold capillary pressure characterizes the ability of a porous medium saturated with a wetting phase (water) to prevent the penetration of a non-wetting phase (injected fluid). If the pressure of the injected gas exceeds the threshold capillary pressure of the brine saturating the caprock, water displacement takes place and slow Darcy flow of the non-wetting gas is triggered [26,27]. The breakthrough pressure identifies the pressure at which a continuous flow of the non-wetting phase is established across the caprock, and leakage occurs.

Direct measurement of breakthrough pressure is made by injecting gas into a brine-saturated caprock sample and reproducing the drainage phenomenon under storage conditions. A detailed summary of the different laboratory tests adopted to measure breakthrough pressure is reported in Ref. [28]. In the scientific literature, reported experiments were performed using nitrogen, methane and CO_2 as the non-wetting displacing fluid [27,29–33]. Very recently, breakthrough pressures for hydrogen were measured for tight sandstone samples [33]. Correlations between the breakthrough pressure and caprock petrophysical properties like permeability, porosity, and resistivity are also proposed [34]. However, there is a complete lack of experimental data on hydrogen breakthrough pressure values for undisturbed clay-rich caprocks, which typically overlie hydrocarbon reservoirs. Some researchers attempted to fill this gap by modeling the monophasic flow of hydrogen and the multiphase flow of hydrogen and brine in low-permeability formations using experimental data on contact angle and interfacial tension (IFT) for H_2-water systems in various mineralogical environments [5,35–43].

In our paper, we present and discuss laboratory step-by-step experiments conducted to measure the breakthrough pressure of hydrogen on plugs retrieved from the ultra-low permeability, clay-rich caprock named Argille del Santerno Formation [44], which overlies several Italian depleted gas reservoirs currently utilized for natural gas storage but under consideration for conversion into hydrogen storages. We investigated the rock mineralogical composition and the brine salinity because they influence interfacial tension and wettability, which in turn dictate the capillary behavior. The experimental results offer a valuable insight into the ability of the caprock to confine hydrogen underground and contribute to proving that the risk of hydrogen migration through the caprock is not more enhanced than for nitrogen or methane, even at a maximum storage pressure above the original reservoir pressure.

2. Concepts and definitions

The capillary mechanism is one of the main phenomena that explains the hydrodynamic sealing of a caprock. The caprock sealing capacity is determined by the forces acting at the interface between the wetting phase (brine), which saturates the caprock, and the non-wetting phase (originally present or injected gas) in the reservoir. The natural capillary retention pressure, P_C, that prevents the non-wetting phase from entering the low-permeable porous medium is defined as the pressure differential between the in-situ pressure of the gas phase (P_{nw}) and the in-situ pressure of the water phase (P_w) above the gas at the gas-water interface [26,45]. Based on the Young Laplace equation (eq. (1)) [46] describing the multiphasic flow of two immiscible fluids in a single capillary tube, the P_C is driven by the interfacial tension (IFT), σ, between the gas and the brine and by the contact angle, θ, formed by the denser fluid phase (water or brine) when adhering to the solid phase (the rock), and is inversely proportional to the equivalent pore radius, r:

$$P_C = P_{nw} - P_w = \frac{2\sigma \cos\theta}{r} \quad (1)$$

Gas flow can occur only if the pressure of the gas phase exceeds the P_C, which explains the ability of a sealing rock to prevent the intrusion and flow of the injected gas.

Hildenbrand et al., 2002 [47] described the stages of the capillary gas breakthrough process in a brine-saturated porous medium. Once the non-wetting phase overcomes the minimum displacement pressure that corresponds to the largest interconnected pore throats and micro-fissures in the medium, it begins to intrude into the porous medium. At this point, the injected gas prioritizes flow paths along the largest interconnected pores that offer the least resistance to intrusion and expels the wetting brine. As the pressure increases, flow is forced in smaller pores and additional flow paths are opened. The breakthrough of the non-wetting phase occurs when a continuous non-wetting phase forms along a series of interconnected pore channels, enabling slow Darcy flow through the medium [27,47].

In a slow displacement, pore filling is controlled by the local capillary pressures [46]. Fig. 1 illustrates a non-wetting phase advancing from one pore to another through subsequent pore throats of different radii. Initially, the differential pressure across the system is lower than the equivalent capillary pressure at pore throat r1, preventing the gas from flowing from pore 1 toward adjacent pore 2. When the threshold pressure is exceeded by a progressive increase in the differential pressure, the gas straddles the throat. Then the non-wetting gas phase continues a slow gas flow across the pore, displacing the brine, until it reaches a pore throat with a smaller radius, r2, necessitating a higher threshold pressure. A further increase in the gas pressure is then needed for the gas to go beyond the pore throat and reach pore 3. Thus, during primary drainage in a complex interconnected pore space, fluid displacement is restricted by narrow sections within the pores, i.e., capillary pressure increases in stages as each narrow “throat” region is gradually filled.

In the technical literature, various definitions exist to denote the characteristic gas pressures describing the capillary sealing efficiency, depending on the stage of fluid displacement or the specific experimental method used [28,47]. In this paper, we refer to the entry pressure as the pressure at which the gas (i.e. the non-wetting phase) first begins to enter the largest pores and to displace the brine (e.g., the wetting phase) [47,48] and to the threshold pressure [26,34], or breakthrough pressure [45], as the pressure at which the gas forms a continuous phase within the porous medium, allowing it to flow. Breakthrough pressure serves as a macroscopic indicator of the sealing capacity of a caprock formation [49].

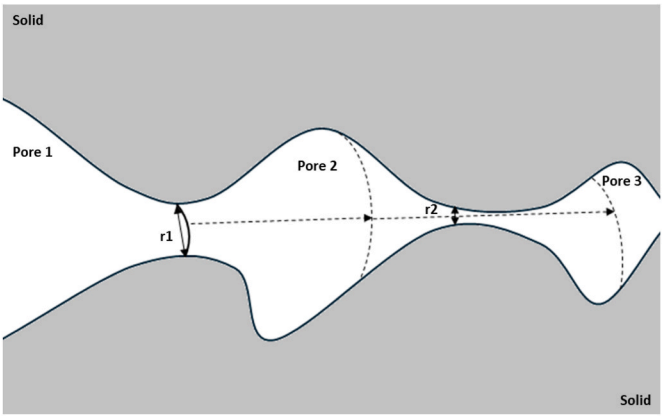

Fig. 1. Illustration of the non-wetting gas phase advancing from one pore to another by overcoming the local capillary pressure (from Blunt, 2017 [46]).

2.1. H_2 interfacial tension and contact angle

As previously recalled (eq. (1)), the interfacial tension (IFT) between the fluids and the contact angle play a critical role in determining the capillary magnitude and thus the caprock effectiveness in confining the gas injected in the underlying reservoir, and several studies have highlighted the need to reassess caprock integrity when repurposing depleted hydrocarbon reservoirs for gas storage. However, studies to determine hydrogen-water/brine IFT and contact angle, and their sensitivities to variables such as pressure, temperature, salinity, and salt species, mineralogy in H_2-brine systems, are relatively scarce, and results are not always fully aligned. This is primarily due to the challenges associated with conducting these experiments under storage conditions, namely at high pressures and temperatures [36]. The pioneering experimental work of Slowinski et al. (1957) [50] and Massoudi & King (1974) [51] reported a larger IFT between pure water and hydrogen than with methane or nitrogen at ambient temperature and showed that the IFT of a water-hydrogen system decreases only slightly with increasing pressure. Other investigations confirmed that the IFT of H_2-brine/water systems is poorly sensitive to pressure, while it varies appreciably with increasing temperature; furthermore, it increases with increasing brine salinity [5,36,38,39,52–55]. Conversely, recent measurements of IFTs between hydrogen, methane, or nitrogen and brine have shown that the IFT between water and hydrogen is lower than those of methane and nitrogen [33,41].

The work of Yekeen et al. (2022) [56], who calculated the IFT between hydrogen and clay minerals (namely kaolinite, illite and montmorillonite) under storage conditions and reported no variations with increasing pressure, suggests that the interactions between hydrogen and clay minerals are quite low; thus, the caprock is expected to remain water-wet during underground hydrogen storage. Furthermore, the contact angle, which depends on the tested substrate, indicates that clay and shale substrates have a strong affinity to water. Their results are in agreement with Al-Yaseri et al. (2021) [52], who obtained contact angles always lower than 40° for kaolinite, illite and montmorillonite under storage conditions (temperature of 333 K and pressures of 5, 10, 15, and 20 MPa) very similar to those of the Italian storages. According to Hosseini et al. (2022b) [5], in carbonate rocks, the contact angle increases with increasing pressure, implying a decrease in wettability, but the opposite occurs with increasing temperature. The experimental results of Al-Mukainah et al. (2022) [36] showed that in shales, the contact angle values also slightly decreased when pressure increased. Conversely, experimental results by Esfandyari (2022) [57] show that the contact angle slightly increases with increasing temperatures for all rock types.

Furthermore, the experimental work done by Hosseini et al. (2022a) [38] and Janjua et al. (2024b) [58] indicates that in calcite-rich formations, both the hydrogen-brine IFT and the contact angle (although slightly) increase with increasing brine molarity under representative storage conditions.

2.2. Experimental assessment of breakthrough pressure

Over the last 70 years, various laboratory techniques, which are generally categorized into direct and indirect methods, have been developed and adopted to quantify threshold pressures [28]. The most common indirect method is Mercury Injection Porosimetry (MIP) [28,31,47]. This approach is widely used because it doesn't require core plugs and can be performed on cuttings. However, MIP has several limitations [59], the main one being the lack of data to convert the mercury-based threshold pressure into a gas-based threshold pressure. Furthermore, it cannot be performed on caprock samples under in situ conditions. As a result, it consistently underestimates breakthrough pressure values [27,60,61].

The direct measurements of the threshold pressures involve the displacement of the wetting phase by a non-wetting phase by injecting gas into brine- or water-saturated plugs obtained from the caprock to be investigated. Ideally, a gas with the same composition as the one to be stored is to be used. The measurements are performed under reservoir thermodynamic and stress conditions.

The step-by-step method was introduced by Thomas et al. (1968) [34] to estimate the breakthrough pressure, and it is the standard direct approach for gas breakthrough experiments. Its main drawback is the need to apply small pressure increments to avoid the overestimation of breakthrough pressure and the extended time required for pressure stabilization at each step.

Less time-consuming procedures were also developed, namely the residual capillary approach [47] to estimate the residual capillary pressure at the end of the test, which is interpreted as a capillary pressure recorded at the end point of the imbibition curve (Fig. 2), and the dynamic threshold pressure approach [60] to determine the entry pressure. However, while these values can provide an idea of the expected caprock sealing potential, they are not representative of the true sealing efficiency of the caprock, as they underestimate the in-situ breakthrough pressure, as can be observed from Fig. 2.

The residual threshold pressure approach provides a conservative value, which is estimated to be 20% to 50% of the breakthrough pressure [53,62,63]. In the dynamic method, entry pressure is influenced by the local heterogeneity of the sample [60] and requires prior knowledge of the expected entry pressure. If the applied pressure gradient is not sufficiently close to this value, achieving capillary equilibrium becomes highly time-consuming, particularly for ultra-tight samples, necessitating precise pressure control and continuous monitoring.

3. Breakthrough pressure experimental setup

We have developed a custom-made experimental setup to perform step-by-step experiments and estimate the breakthrough pressure to hydrogen. The test also provides the entry pressure. The customized threshold pressure setup, shown in Fig. 3, consists of a high-pressure core holder fitted with a thick rubber sleeve to confine the rock plug. Upstream, a high-precision injection syringe pump, capable of handling both gases and liquids, can operate either in a pressure control or in a flow rate control mode. The wetted parts of the system are made in Hastelloy, ensuring safe operation with hydrogen. Downstream, a back-pressure regulator (BPR) controls the outlet pressure. A manual hydraulic pump is used to apply the confining pressure within the core holder. The instrument offers operational pressure ranges from 0 to 700 bars.

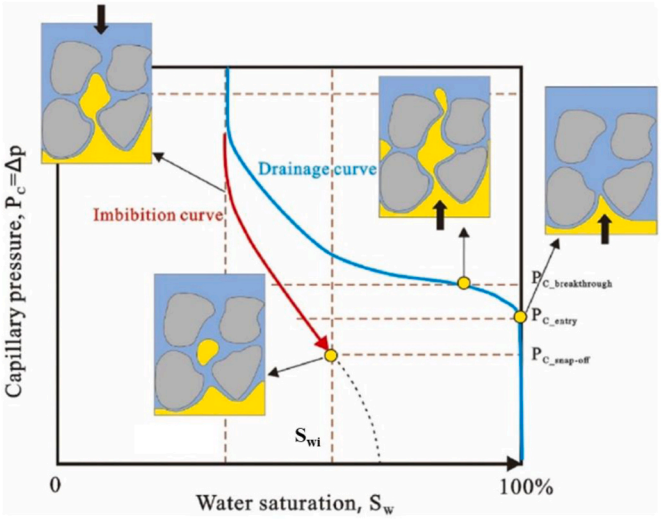

Fig. 2. Capillary pressure values during drainage and subsequent imbibition [28].

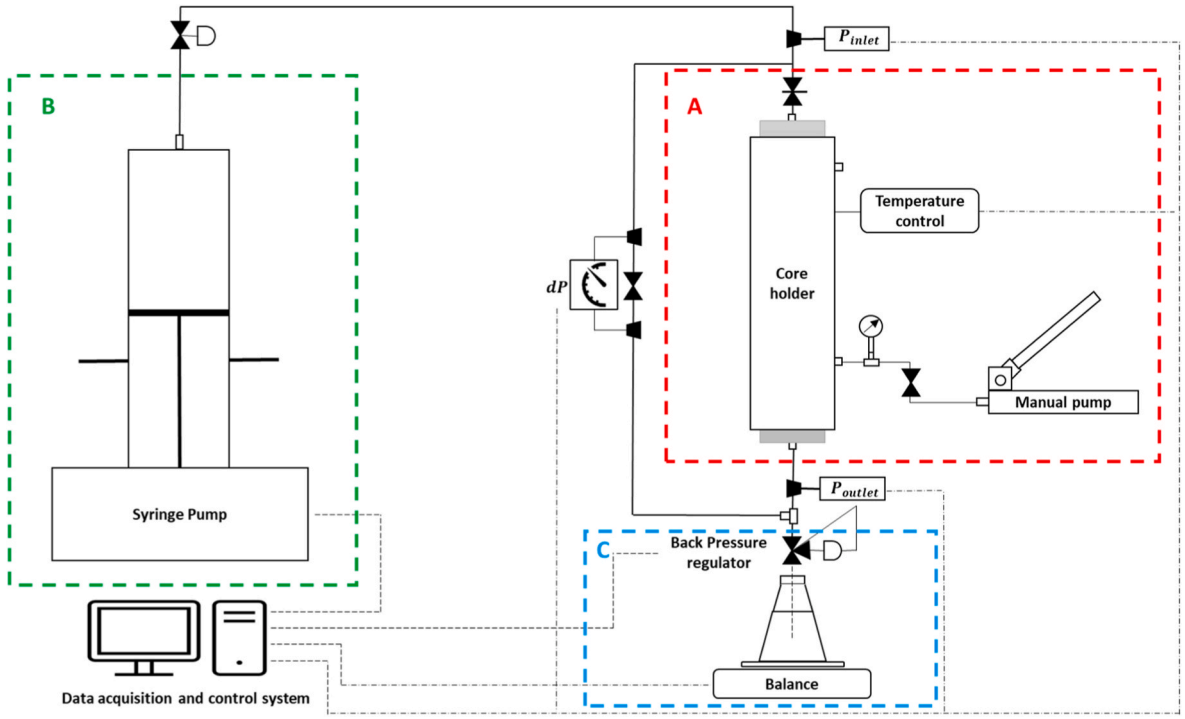

Fig. 3. Schematic of the threshold pressure experimental setup. A: Core holder system, B: Upstream system: Syringe injection pump, and C: Downstream system: collection tank + balance + digital camera.

Three pressure transducers monitor the inlet pressure, outlet pressure, and pressure difference across the core holder. Pressure measurement accuracy is ±1 psi, while the achievable flow rates range from 0.05 ml/min (8×10^{-10} m^3/s) to 94 ml/min (1.6×10^{-6} m^3/s). The core holder can accommodate standard plugs with a 1.5" (38.1 mm) diameter and varying lengths.

The system outlet feeds into a tank filled with transparent ISOPAR oil through a vertical 5-cm long transparent capillary tube with a 1/16 inch diameter OD (1.53 mm), which is observed with a digital camera. This allows the visual differentiation between leaked-off fluids, brine or gas, based on their different buoyancies in oil. The tank is set on top of a sensitive balance to record any mass variation observed due to brine production. The entire apparatus is connected to a computer acquisition system that monitors and records key parameters, including pump injection pressure and injection flow rate, pressures at the inlet and outlet of the core holder, and the differential pressure across the plug.

4. Materials and testing

Three cores were drilled from the "Argille del Santerno" geological formation in the western Po Plain, Northern Italy. The caprock "Argille del Santerno" formed during a tectonic episode that affected the entire Apennine fold-and-thrust belt. This event caused rapid subsidence in the foreland areas, leading to a marine transgression and the extensive deposition of marine clays across large portions of the foreland. The Argille del Santerno formation has been the object of numerous investigation surveys, often related to hydrocarbon reservoir targets and conversion of depleted reservoirs into natural gas storage. The formation is a good-quality, continuous shale, without faults or fractures [64].

Although belonging to the same formation, the caprock cores were identified as Caprock 1 and Caprock 2 because they were retrieved from two different locations, approximately 40 km apart.

For Caprock 1, two cores were collected from nearby wells, Well A and Well B, intersecting the "Argille del Santerno" formation from an interval at a depth of approximately 1257-1264 m TVD ss and 1396-1398 m TVD ss, respectively. Both cores were enclosed in aluminum liners, sealed by plastic end caps, and stabilized with gypsum in the annular space to prevent any alteration of the rock during transport and storage. The cores were delivered to the lab for plug preparation.

For Caprock 2, plugs were obtained from a single core collected at Well D, at a depth of 1285-1287 m TVD ss, were encapsulated in rubber sheaths and aluminum to maintain their original brine saturation, and delivered to the lab ready to be tested.

While natural fractures were not to be expected, X-Ray Computed Tomography was performed on both the cores and plugs to detect microfissures and cracks potentially induced by drilling, core extraction from the core-holder, or partial drying of the samples.

4.1. X-Ray Computed Tomography

Before opening the cores from wells A and B, X-Ray Computed Tomography (CT) was performed to evaluate the quality and integrity of the cores. The resulting CT scan images were analyzed to identify the most homogeneous sections for plug sampling, focusing on the orientation of laminations and the presence of microfractures that could affect the sampling process and test results.

4.2. Plug sampling process

The "Argille del Santerno" caprock contains a high percentage of soft clays that are easily broken by mechanical stress. Conventional coring tools are problematic because the rapid rotation of the coring tool generates heat, which can alter the clay and compromise the structure of the porous material. Thus, water is generally used to cool both the machine and the point of contact with the rock. However, low-salinity water can cause the clay to swell, further disrupting the porous structure. Additionally, the rapid application of a uniaxial load on the sample can lead to tensile failure at its base. Therefore, a dry process, typically used for loose soils, was adopted to minimize rock alterations and tensions on the core. The Soil Die Cutter, shown in Fig. 4, provides a less aggressive approach to plug retrieval. The Soil Die system presses a hollow cylindrical die-cutter into the core to extract a plug. It cuts

Fig. 4. A) isolated core segment placed inside a Soil Die Cutter. B–C-D) downward manual pressing of the cutting die through the core while carving the surrounding material away from the plug from the core.

through the core by lowering a cutting die step by step, 1 to 2 cm each step, to penetrate the core, and the core is carved manually around the cutting die as the tool advances.

The collected plugs, approximately 1.5″ in diameter and 3" in length (except for 2 shorter ones), were sealed inside a sheath and placed inside a thermostatic (6 °C) humid chamber to preserve their original saturation.

4.3. X-Ray Computed Tomography on plugs

X-ray Computed Tomography (CT) was performed to evaluate the quality of the plugs obtained from Well D. The resulting CT scan images were analyzed to identify the best plugs, focusing on the presence of microfractures that could affect the test results.

An example of the CT scan images is shown in Fig. 5.

4.4. Tested caprock plugs

In total, a set of 9 plugs from all the cores (Wells A, B and D) was available for subsequent testing (see Table 1).

4.5. Caprock particle size analysis

The particle size analyses were performed using the by-product from plug sampling from the two cores from Wells A and B and the core from Well D. Thus, we made 3 particle size analyses.

Based on the standard practice for the classification of soils for engineering purposes: Unified Soil Classification System (USCS) – ASTM D2487-10 [65], initially, we separated the coarse from the fine-grain material using the 75-μm sieve. For the coarser fraction, sieve analysis – ASTM D6913-04 [66] was performed, mechanically separating particles by passing them through a series of finer sieves to determine the gradation of sand. Fine particles were analyzed using a hydrometer test – ASTM D7928-17 [67], which involves treating the material with sodium hexametaphosphate for 12–16 h to prevent coagulation. The sample was then suspended in distilled water, and sedimentation rates were measured with a hydrometer to determine the proportions of silt and clay.

The obtained results, summarized in Table 2, show that the caprock is dominated by clay-size and silt-size particles, with a negligible quantity of sand particles (less than 1%). Caprock1 consistently exhibits approximately 64% of clay and 35% of silt by weight (the same results were obtained for the rock coming from the two nearby wells). Caprock2 contains comparable percentages of silt and clay. In both cases, due to their high clay and silt content, the samples are classified as mudrocks [68].

Table 1
Caprock plugs.

Caprock	Well	Sample ID	Depth (m TVD ss)	Length (cm)	Diameter (cm)
Caprock 1	A	A1	1257.55	7.64	3.82
	A	A2	1260.33	7.66	3.79
	A	A3	1263.10	7.67	3.73
	B	B1	1396.50	7.60	3.80
Caprock 2	D	D1	1285.53	7.68	3.74
	D	D2	1285.62	7.72	3.74
	D	D3	1285.94	5.72	3.74
	D	D4	1285.94	3.71	3.75
	D	D5	1286.10	8.12	3.76

Table 2
Particle size composition.

Caprock	Well	Clay content (% weight)	Silt content (% weight)	Sand content (% weight)
Caprock 1	A	64	35	<1%
Caprock 1	B	64	35	<1%
Caprock 2	D	50 - 55	44 - 49	<1%

4.6. Caprock X-ray diffraction (mineralogical composition)

The mineral composition of the caprocks was assessed using X-Ray diffraction on material obtained from the cores from wells A, B and D. Mineral classes were identified based on their main weight percentages obtained via Rietveld refinement analysis [69]. To enhance the

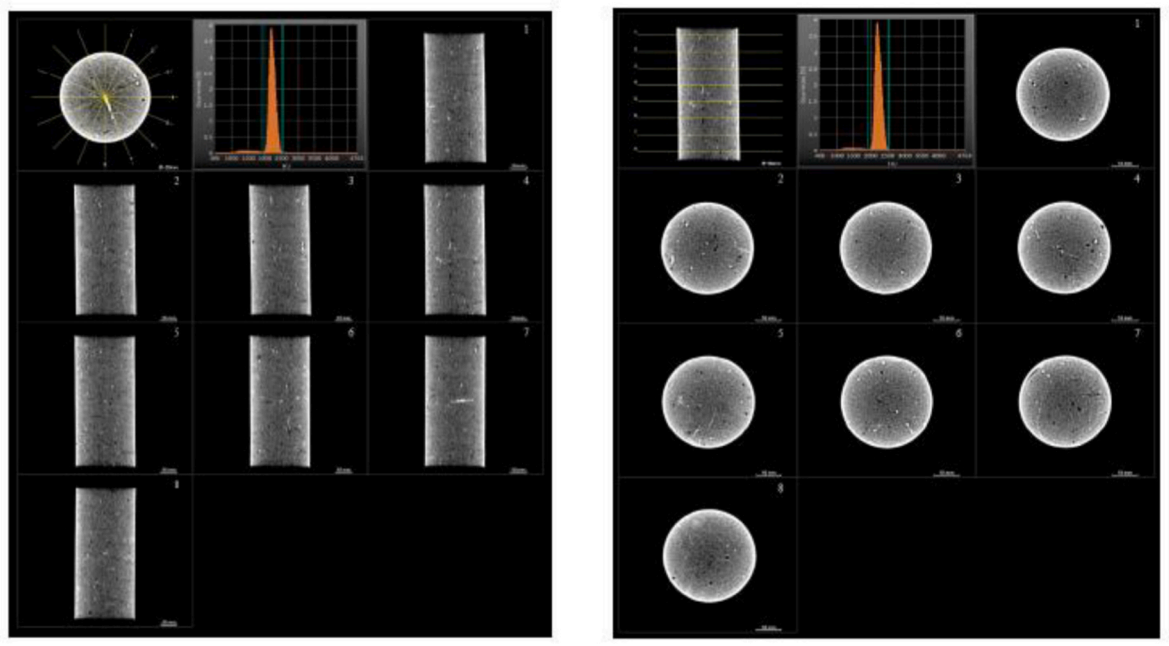

Fig. 5. Longitudinal and cross-sectional CT images of plug D5.

compositional representativeness and statistics, three samples were selected from each core to provide a robust characterization of the local mineralogy. Detailed procedures for X-Ray diffraction and performed analyses are documented in Chiodoni et al. (2024) [70]. Results are reported in Table 3.

The mineralogical analysis of the caprock revealed a consistent compositional profile across equivalent intervals. Variations observed between specimens are attributed to natural rock heterogeneity. Quantitative results indicate that the caprock samples are predominantly composed of carbonate minerals, primarily calcite and dolomite. Samples from Well A exhibit a more calcareous composition than samples from Well B. In contrast, Caprock 2 (Well D) contains less calcite and a higher proportion of dolomite. Quartz is the dominant tectosilicate, while illite is the most prevalent clay mineral.

4.7. Brine hydro-chemical analyses

The brines collected from the reservoirs below Caprock 1 and Caprock 2 were subject to a hydro-chemical analysis to evaluate their composition. Three descents of fluids were collected at Well A and Well D and analyzed independently. The obtained average salinities are provided in Table 4.

4.8. Step-by-Step threshold pressure tests with nitrogen

Results from step-by-step tests performed with nitrogen on plugs obtained from cores adjacent to Well A (Caprock 1) and Well D (Caprock 2) were made available as a reference by Snam-Stogit. Before testing, the unpreserved plugs had been re-saturated with high-salinity brine with 110′126 ppm of NaCl. The breakthrough pressure values for nitrogen are summarized in Table 5.

Threshold pressure values below 20 bars are likely not representative. Such low values are probably due to the presence of microfractures, potentially induced during coring operations and/or plug preparation, or due to low water content resulting from poor preservation or re-saturation. Thus, representative breakthrough pressures to nitrogen (N_2) range from 20 to 35 bars for Caprock 1 and from 30 to 45 bars for Caprock 2.

4.9. Step-by-Step threshold pressure tests with hydrogen

To measure breakthrough pressure with hydrogen, we adopted the step-by-step method. The method involves increasing the pressure gradient across the plug in steps by injecting gas and allowing a stabilization period at each step while monitoring downstream fluid leak-off, i.e., the gas and/or brine production or lack thereof. The process continues until the first bubble of injected gas is observed downstream, indicating gas breakthrough. This breakthrough implies that the non-wetting gas phase has formed a continuous phase across the sample, displacing the brine and allowing gas to flow under Darcy conditions.

Each preserved plug was placed inside the core holder between two end-sample seats. These seats were designed with evenly spaced geometric lines to ensure a uniform distribution of gas pressure across the faces of the samples during testing.

The testing conditions were chosen so as to be consistent with the step-by-step tests conducted with nitrogen (Table 5) and to compare the confinement efficiency of the investigated caprock to hydrogen relative to nitrogen. Thus, the temperature was maintained at ambient temperature (20 °C) and all the tests were performed without the application of a back-pressure.

In our tests, the confining pressure was increased incrementally until 90 bars were reached to replicate in-situ stress conditions and prevent lateral gas leakage. The inlet pressure was increased incrementally and held steady at each step using the pressure control mode of the syringe pump, while the outlet pressure remained constant. At each pressure increment, both the upstream pump volume and the outlet flow were closely monitored. The upstream pump volume must remain stable

Table 4
Brine salinities obtained from hydro-chemical analysis performed on samples taken from the reservoirs overlayed by Caprock 1 and Caprock 2, respectively.

Salinity	NaCl (ppm)	$CaCl_2$ (ppm)
Reservoir 1	56′896	11′782
Reservoir 2	53′560	23′701

Table 5
Experimental breakthrough pressure values for nitrogen.

Caprock	Sample ID	Injected gas	Depth (m TVD ss)	Breakthrough Pressure (bars)
Caprock 1	P1	N_2	1257.98	15
	P2	N_2	1261.32	10
	P3	N_2	1261.82	20
	P4	N_2	1265.26	15
	P5	N_2	1270.14	15
	P6	N_2	1271.92	35
Caprock 2	M1	N_2	1284.56	40
	M2	N_2	1286.33	45
	M3	N_2	1286.42	10
	M4	N_2	1287.53	45
	M5	N_2	1287.73	35
	M6	N_2	1287.74	35
	M7	N_2	1289.91	40

Table 3
Mineralogical content obtained from the Rietveld analyses.

Minerals		Composition (weight %)		
		Caprock 1		Caprock 2
		Well A	Well B	Well D
Tectosilicates	Quartz	24.0 - 25.4	16.2 - 17.9	14.4 - 19.9
	Plagioclase (albite. anorthite)	7.2 - 9.1	5.7 - 6.5	5.1 - 8.0
	K-feldspar	9.3 - 9.7	7.6 - 8.2	6.2 - 7.3
	Group content	*41.0 - 43.9*	*30.9 - 33.2*	*28.2 - 32.3*
Carbonates	Calcite	32.5 - 33.8	40.3 - 48.1	26.8 - 30.0
	Dolomite	7.4 - 8.1	3.7 - 6.7	17.5 - 20.8
	Siderite	0	0	0.5 - 0.7
	Group content	*40.4 - 41.9*	*47.0 - 54.0*	*46.9 - 48.5*
Phyllosilicates (Clay minerals)	Illite	6.3 - 10.9	7.5 - 15.0	11.3 - 20.7
	Chlorite	3.5 - 3.8	2.2 - 3.2	2.9 - 4.4
	Kaolinite	2.6 - 3.1	3.7 - 4.6	2.3 - 3.6
	Group content	*12.9 - 17.3*	*14.5 - 21.9*	*18.6 - 24.4*
Other minerals	Pyrite	0	0 - 0.3	0.3 - 0.4
	Halite	1.1 - 2.4	0	0.1 - 0.3

under constant pressure. The syringe pump tracks the gas volume by the piston position, and when the inlet pressure is adjusted, the piston compresses the gas accordingly. Under stable temperature conditions, this volume remains unchanged. However, as gas approaches the displacement pressure, the pump volume may exhibit a minuscule decrease, suggesting the initiation of gas penetration into the plug. The entry pressure was recorded after the first droplet of brine was produced and verified by the digital camera recording. Breakthrough was confirmed when continuous gas flow was observed downstream, marking the end of the test.

Due to the low permeability of the formation under investigation, the tests were very long. Typically, it took weeks to complete each test, as each pressure increment required from one to several days for the upstream pump volume to stabilize and show negligible or null variations, indicating that the capillary pressure equilibrium had been reached within the plug.

A key factor in accurately estimating the threshold pressure was the selection of the correct delta pressure increment. If the pressure increment is too large, there is a risk of overestimating the breakthrough pressure. Conversely, if the increment is too small, the testing process can become excessively lengthy for a single measurement. Therefore, a compromise must be made between sufficient stabilization time and selecting appropriate pressure increments to ensure that the breakthrough pressure is representative [27,28,60,71]. In our experimental protocol, we set the pressure gradient increments at 5 bars with progressively longer stability periods. Every 3 pressure steps, i.e., 15 bars with no fluid activity detected downstream, an additional day was added to ensure that pressure equilibrium was reached within the pore system. Upon detecting brine downstream, we waited an additional 24 h after the brine leak-off ceased before applying the next pressure increment. When the injected gas was detected downstream, the test was terminated, and the last recorded pressure gradient (ΔP) was taken as the breakthrough pressure.

In Fig. 6, the experiment recordings (pressure difference across the plug and brine production) are shown for one of the tested plugs (plug A3).

Nine Step-by-Step tests were conducted to determine breakthrough pressure. In the first test, we used methane to have a reference result consistent with the gas currently stored in the depleted reservoirs. Due to the risks associated with the use of methane in laboratory experiments, nitrogen is typically used as its proxy in standard practice because of its comparable threshold pressure values [26,29]. In the subsequent 8 tests, we used hydrogen. Two tests were repeated, still using hydrogen, on re-saturated plugs, as the first attempts were not successful, likely due to poor saturation.

Initially, as the injection pressure increased incrementally, no flow was observed downstream. Trapped air appeared sporadically with brine flow, caused by depressurization during core retrieval. When gas started penetrating the plug, there was evidence that the pressure gradient had exceeded the capillary pressure corresponding to the largest effective pore radius at the inlet of the plug and that gas had started to displace the wetting brine. This stage marked the initiation of the drainage process. At this step, brine leak-off may be detected downstream. As the inlet pressure was further increased, periodic brine production was detected, proving that the drainage phenomenon was ongoing. The differential pressure at which the injected gas showed continuous flow through the plug was taken as the breakthrough pressure.

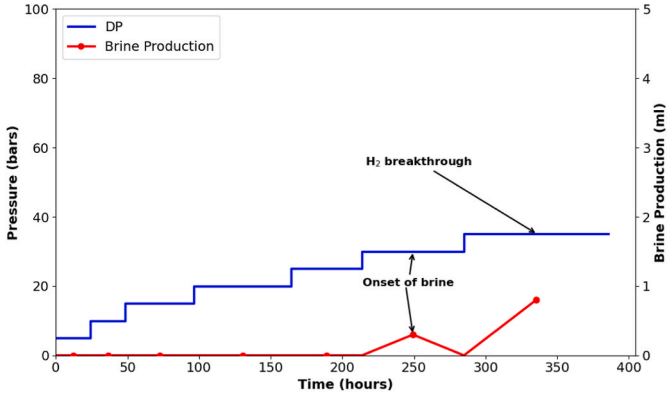

Fig. 6. Differential pressure, DP, profile and brine production recorded during the Step-by-Step test for plug A3.

4.10. Permeability measurements

After the breakthrough was achieved and the injected hydrogen flew continuously through the plug, we assessed the permeability to hydrogen. Since effective permeabilities depend on saturations, we kept flowing gas for 48 h at a higher-pressure gradient than the one applied when gas breakthrough occurred (breakthrough pressure plus 10 bars). This ensured additional brine displacement. When no more brine was detected under further hydrogen flow, constant saturation was assumed and permeability was measured.

The permeability to hydrogen at residual water saturation was calculated using the Darcy equation (eq. (2)) for compressible fluids:

$$k_g = \frac{2\,\mu\,Q\,L\,P_1}{A\left(P_2^2 - P_1^2\right)} \tag{2}$$

where μ is the dynamic viscosity of the injected gas at the testing (ambient) temperature, Q is the upstream gas flow rate recorded through the volumetric variation within the pump at each pressure gradient, A is the cross-sectional area of the plug, L is the length of the plug, and P1 and P2 represent the inlet and outlet pressures, respectively.

5. Results and Discussion

5.1. Breakthrough pressure test results

The obtained entry pressure and breakthrough pressure values, with the testing conditions applied to each plug, are summarized in Table 6.

As introduced in section 4.9, tests were performed at ambient temperature (20 °C) and without application of a back-pressure to enable a direct comparison between hydrogen and nitrogen breakthrough pressures. Based on the literature review (see section 2.1), a temperature increase for calcite-rich clays will likely positively affect the capillary sealing capacity of the caprock, while a pressure increase will adversely affect the threshold pressure. However, even if a slight reduction in the breakthrough pressure measured with laboratory experiments might occur under storage conditions, the caprock is expected to remain water-wet, as confirmed by experiments on clays under similar pressure and temperature conditions [52]. Thus, the obtained results are deemed to be representative despite the lack of back-pressure and the reduced temperature relative to in situ conditions.

Brine detection downstream occurred at pressures 5 to 10 bars lower than the breakthrough pressure for hydrogen and 15 bars lower than the breakthrough pressure for methane. Busch et al. (2013) [72] noted that in small-scale laboratory experiments, it can be difficult to distinguish between entry and breakthrough pressures if the plugs are homogeneous and permeability is not extremely low. Our experiments clearly show this distinction, probably because the plugs are slightly heterogeneous and their permeability is very low. Furthermore, the use of increasingly longer time steps, with the longest recorded at seven days, allowed sufficient time for capillary equilibrium to establish. Consequently, the onset of brine downstream corresponding to the entry pressure could be detected. However, due to the limited brine production at water breakthrough, which was below the sensitivity threshold of the balance,

Table 6
Results of the step-by-step tests.

Caprock	Well	Plug	Injected gas	Confining Pressure (bars)	Entry pressure (bars)	Threshold pressure (bars)	Test duration (days)
Caprock 1	A	A1	N_2	90	-	-	<1
	A	A1 resaturated	H_2	90	20	25	13
	A	A2	CH_4	90	15	30	11
	A	A3	H_2	90	30	35	13
	B	B1	H_2	90	-	-	12
	B	B1 resaturated	H_2	90	70	75	44
Caprock 2	D	D1	H_2	90	65	70	38
	D	D2	H_2	90	60	70	37
	D	D3	H_2	90	40	40	15
	D	D4	H_2	90	>80	>80	55
	D	D5	H_2	90	-	-	<1

quantitative measurements were not feasible and the assessment of brine onset was based on visual inspection of the digital camera footage, when the first droplet of brine was captured on the camera continuously recording the outlet tubing, which has a short length, small diameter and is transparent to minimize uncertainty in the detection (see section 3).

The breakthrough pressure measurements for Caprock 1 range from 25 to 35 bars, independent of the injected gas. Caprock 2 exhibits a wider range of hydrogen breakthrough pressure from 40 bars to values higher than 80 bars. For the test on plug D4, no activity was detected downstream, even when the differential pressure reached 80 bars.

In the case of plug D3, for which the onset of brine and hydrogen breakthrough were recorded within minutes when 40 bars were reached and the produced brine was negligible, and in the case of plugs A1 and D5, for which hydrogen flow was detected as soon as a differential pressure (5 bars) was applied, it is likely that the plugs were not fully saturated. As for plug B1, the hydrogen breakthrough occurred at 35 bars without any water production; this implies that the plug was dry but with very low permeability. Based on the literature, there is a strong correlation between threshold pressure and water content, and breakthrough pressure increases exponentially with water saturation [73,74]. It was inferred that, despite the efforts to preserve the cores after drilling, the plugs were poorly saturated. This might have happened because the cores of Caprock 1 were drilled 5 years before testing. Conversely, the period between drilling of the core from Caprock 2 and lab testing was a few weeks; thus, clay saturation was not expected to be altered, and we inferred that early breakthrough might be due to the presence of microfractures that went undetected during plug inspection with CT-scan.

To verify whether the results on plugs A1 and B1 were affected by poor saturation, as we had hypothesized, we decided to re-saturate them and run the step-by-step test again. The plugs were saturated with synthetic brine mimicking the salinity of the formation water (previously measured with the hydro-chemical analyses). Under the same testing conditions outlined in par. 4.9, the brine was injected into the plugs by increasing the pressure in steps while monitoring the downstream activity. Brine pressure was increased by 5 bars at the time, after no volume variation of the pump was monitored for at least 12 h. When brine was detected downstream, an additional 48 h of brine flooding were conducted to ensure the saturation of the plugs.

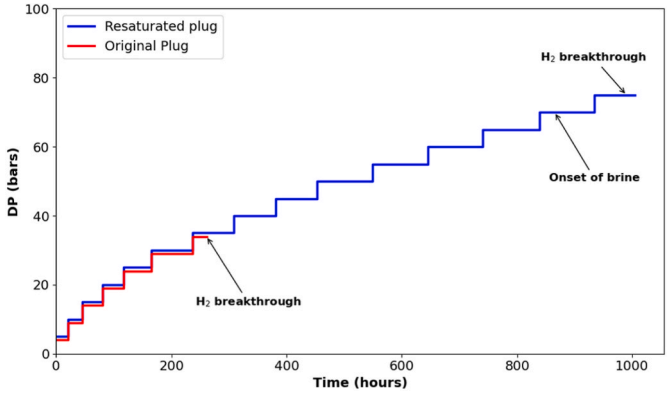

Fig. 7. Step-by-Step test with hydrogen for plug B1 before and after re-saturation.

The step-by-step tests on the re-saturated plugs, conducted under the same conditions as the previous experiments, revealed a brine onset at 20 bars for plug A1 and 70 bars for plug B1. Hydrogen breakthrough occurred at 25 bars and 75 bars, respectively. These results confirmed that the failure observed in the original tests was due to dried-out conditions, which affected the sealing capacity of the plugs (see Fig. 7). The results are also shown in Table 6.

Recent literature addressed the impact of cyclic pore-pressure variations or cyclic loading and unloading on the sealing performance of clays and shales [75–77]. While these works do not directly correlate with our study because of the adopted experimental methodology [77] and the experimental focus on the rock mechanical deformation and integrity [75,76], they stimulate interest in investigating whether the storage cycles have any effects on threshold pressure.

5.1.1. *Impact of caprock mineralogical composition*

Fig. 8 shows the measured hydrogen breakthrough pressure as a function of the caprock composition (range of weight percentage for each mineral group). Even if data is limited, this analysis reveals weak correlations between hydrogen breakthrough pressure and carbonate content (Fig. 8A), clay minerals content (Fig. 8B) and tectosilicate content (Fig. 8C), respectively: higher breakthrough pressure values correspond to slightly higher carbonate and clay minerals content and to lower tectosilicate content; these qualitative correlations are in line with the results provided by Zhou et al. (2022) [78], who also inferred a direct correlation between methane breakthrough pressures and carbonate content, particularly calcite, while dolomite appeared to have little to no effect.

Only a few studies that determined the IFTs between hydrogen and rock minerals can be found in the literature. The reported values seem to indicate some variability based on mineral composition. Esfandyari et al. (2023) [79] determined interfacial tensions between hydrogen and minerals in the presence of distilled water at 10 bars and at 20 °C, in the following order: dolomite 94 mN/m > quartz 82 mN/m > calcite 76 mN. Similar values have been calculated for calcite (90 mN/m at 25 °C and 50 bars) by Hosseini et al. (2023) [80] and for aged quartz (90 mN/m at 50 °C and 100 bar) by Pan et al. (2021) [81]. Based on the work by Hosseini et al. (2022b) [82], comparable IFTs (75 mN/m at 50 bars and 25 °C) were obtained between hydrogen and three shales characterized by various mineralogical compositions (Shale A: 61% carbonates, 28% clay minerals; Shale B: 31% tectosilicates, 62% clay group minerals; and Shale C: 25% tectosilicates, 55% clay group minerals). Similarly, Yekeen et al. (2022) [56] estimated the IFT between hydrogen and illite, kaolinite and montmorillonite to be approximately 70 mN/m at 60 °C

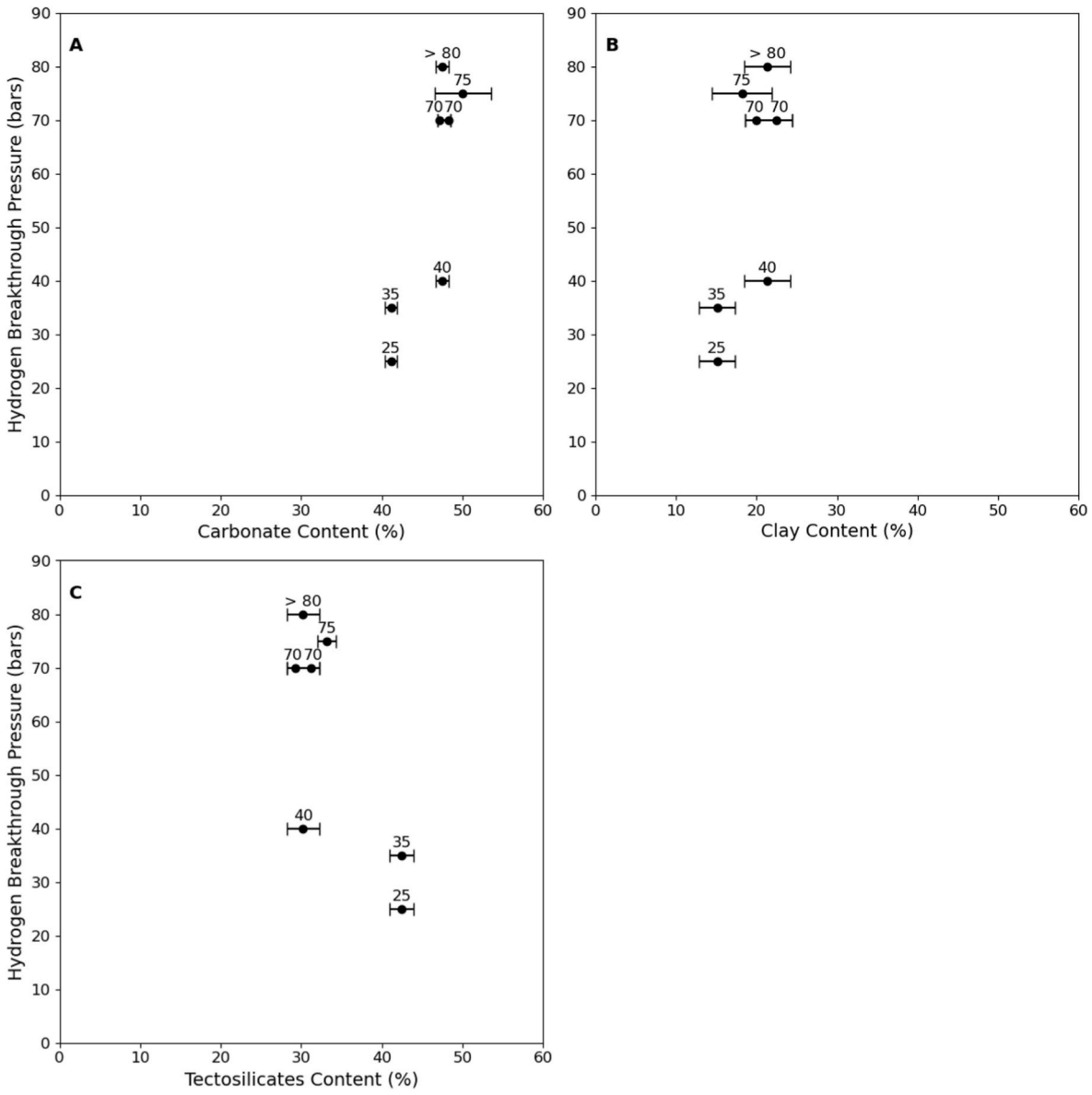

Fig. 8. Hydrogen breakthrough pressure (bars) as a function of the weight content (%) of: A-carbonates, B) Clay minerals and C) Tectosilicates.

and 50 bars.

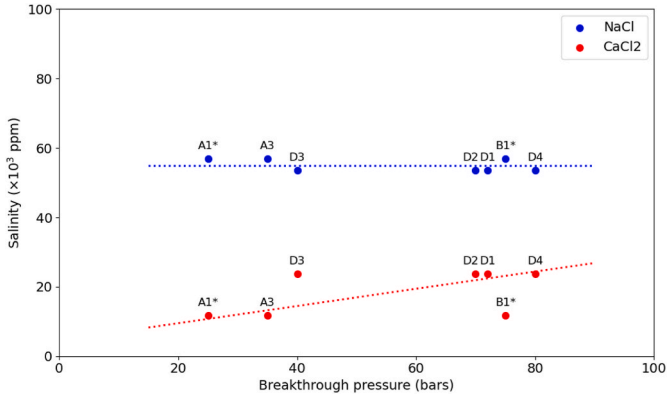

Fig. 9. Hydrogen breakthrough pressures against NaCl and $CaCl_2$ concentrations [samples labeled with an asterisk (*) were re-saturated with synthetic formation brine].

Hydrogen-brine contact angles, measured for different minerals at different pressures and temperatures, are available in Esfandyari et al. (2022) [57]. They found that the contact angle values decrease with increasing pressure and temperature, but the variations due to pressure change were higher than those due to the temperature change. The experiments on the shales reported in Hosseini et al. (2022b) [83] show that all the shale substrates have a strong affinity to water, with all the measured contact angles being lower than 30° under the same conditions. Therefore, the systems are strongly water wet.

5.1.2. *Impact of salinity*

Fig. 9 displays the hydrogen breakthrough pressures as a function of the brine salinity for the preserved plugs from caprock 1 and caprock 2, and the re-saturated plugs A1 and B1. As previously reported, the formation brines of both caprocks exhibit comparable NaCl concentrations but different $CaCl_2$ concentrations (Table 4). Qualitatively, the data seem to confirm a direct correlation between the measured hydrogen breakthrough pressure and the $CaCl_2$ concentration in the brine, except for plugs B1 and D3, which do not align with the general trend. Our results are consistent with previously published studies, where trends

indicate a linear increase in the H_2-brine interfacial tension with increasing salinity and bivalent cation content, namely $CaCl_2$ [38,41,57,84].

5.2. Permeability measurements

The permeability tests to obtain the effective permeability to gas, k_g, at residual water content were performed on plugs A2, A3 and D3, which were the most suited based on the relatively low threshold pressure values that were measured. Plugs B1 and D5 were deemed inadequate because they were likely dry and fractured, respectively. The remaining plugs were too tight to permit sufficient gas flow for permeability calculation, requiring several days to observe any volumetric variation at the pump level.

Hydrogen was injected into the three selected plugs under increasing pressure gradients ranging from 40 to 70 bars. The resulting flow rates (approximately 2 10^{-12} m^3/s) were below the sensitivity threshold of the pump (2 × 10^{-11} m^3/s). Consequently, flow rates were determined based on volumetric variations recorded at the pump every 5 min.

The calculated permeability values are reported in Table 7. The caprock plugs exhibited ultra-low permeability, and no correlation with the measured breakthrough pressures is possible.

Experimental work on an intact sample of Marcellus shale subject to cyclic pore-pressure variations showed a progressive volumetric swelling of the shale matrix, with an observed 12% porosity increase after eight cycles and an estimated 19% porosity increase after 30 cycles [85]. Although the study is very interesting because it attempts to assess the effects induced on caprocks by the cyclic pressure variations in the underlying reservoir, it is noted that the experiment was performed on an unconstrained shale sample. Thus the porosity variations are overestimated because the experimental conditions are not representative of in-situ conditions, where pressure variations only apply at the interface between the caprock and the reservoir. Furthermore, the Ajibona and Pandey [85] expect that permeability, estimated according to the Kozeny-Carman relation, might increase by 70% due to such porosity increase. However, the Kozeny-Carman relation is not suited to estimate permeability in the case of anisotropic rocks, heterogeneous pore distribution, multiphase flow and presence of capillary effects, which is exactly the case of clay-rich rocks.

5.3. Nitrogen vs hydrogen breakthrough pressure

Fig. 10 illustrates the comparison of breakthrough pressures measured for hydrogen, methane, and nitrogen under the same testing conditions (20 °C and no back-pressure). The breakthrough pressures of the tested plugs are plotted as a function of the sampling depth. No dependency emerged between the type of injected gas and the measured breakthrough pressure, as for caprock 1 hydrogen exhibited breakthrough pressures in the range of 25–70 bar, methane 30 bar, and nitrogen between 20 and 35 bar while for Caprock 2 hydrogen breakthrough pressures range from 40 bar to values exceeding 80 bar and nitrogen breakthrough pressures range from 35 to 45 bar. Differences in the measured breakthrough pressure values are believed to depend on local variations of the rock mineral composition, because all the plugs are made of undisturbed rock and exhibit small heterogeneities, as highlighted by the mineralogic analyses, even if they were taken from the same Argille del Santerno caprock formation at approximately the same depth. This could also explain the peak values of 70 bars or more for some of the measured hydrogen breakthrough pressure values.

In the literature, some attempts have been made to correlate the breakthrough pressure with the gas-brine IFTs. According to the most recent literature, at ambient conditions, the IFT between distilled water and hydrogen is reported as 70,91 mN/m [41], while those with nitrogen and methane IFTs are provided by Yan et al. (2001) [86] and Ren et al. (2000) [87] and equal to 71,43 mN/m and 72,96 mN/m, respectively. Li et al. (2025) [33] report that, at ambient conditions, the average interfacial tensions between the brine (total salinity 74′000 ppm) and H_2, N_2, CH_4 are 71,57 ± 0,28 mN/m, 72,11 ± 0,31 mN/m and 72,03 ± 0,53 mN/m, respectively; their experimental breakthrough pressures for tight sandstones, with hydrogen breakthrough pressure being lower than that of methane and nitrogen, slightly reflect the corresponding IFTs values. However, opposite results were reported by Slowinski et al. (1957) [49] and Massoudi & King (1974) [50] for hydrogen-water/brine IFT. Most importantly, hydrogen-quartz IFT is larger than the hydrogen-clay IFT, and hydrogen-clay IFT appears to be larger than those of natural gas and carbon dioxide, suggesting that a brine-saturated clay-rich caprock formation should offer more effective capillary sealing to hydrogen than to other fluids [56,81]. Furthermore, the contact angle, which significantly contributes to capillary retention, appears to be smaller for clays [52] than for quartz [88] or very similar [57] under high-pressure conditions. Therefore, the correlation between brine-gas IFT and breakthrough pressure might have a limited validity, and the results obtained from testing sandstones rather than clay-rich caprocks might be misleading in assessing the sealing efficiency of a real caprock.

Table 7
Calculated permeability values.

Caprock	Plug ID	Injected gas	Permeability (nD)
Caprock 1	A2	CH_4	<1
	A3	H_2	<1.5
Caprock 2	D3	H_2	<1.6

6. Conclusions

We conducted a set of 9 step-by-step experiments to measure the threshold pressure to hydrogen on plugs retrieved from the caprock named “Argille del Santerno Formation”, which is a clay-rich formation with ultra-low-permeability overlying several Italian depleted gas reservoirs currently utilized for natural gas storage but under consideration for conversion into hydrogen storages. To the best of the authors’ knowledge, these are the first reported experiments of breakthrough pressure measurements with hydrogen on plugs obtained from a real caprock. The step-by-step experiments were performed with a confinement pressure of 90 bar and at ambient temperature (20 °C) for the sake of consistency with previous breakthrough pressure experiments performed with nitrogen on plugs collected from the same caprock, so as to ensure a meaningful comparison between the breakthrough pressure values obtained for nitrogen and for hydrogen. One test with methane was also performed under the same conditions for comparison.

The experimental results showed that the values of breakthrough pressure to hydrogen, nitrogen and methane are comparable, with no evidence that the caprock sealing capacity decreases when hydrogen is the displacing gas. The mineralogical analyses showed some heterogeneity of the caprock from which the plugs were sampled, namely some variability in the calcite, clay minerals, and tectosilicate content; consistently with the literature, higher threshold pressure values correlate to larger carbonate and clay content. Hydrochemical analyses on the formation waters sampled from the reservoirs below the caprock were also performed; the results seem to confirm that breakthrough pressures increase for increasing $CaCl_2$ content.

Based on the scientific literature, the hydrogen-brine interfacial tensions slightly decrease when the pressure increases, while it is uncertain whether the contact angle will slightly increase or decrease, as opposite trends have been experimentally observed for shales. Similarly, the gas-liquid interfacial tensions are expected to decrease when the temperature increases, while contact angles are reported to slightly increase but also to decrease in some calcite-rich rocks and clayey rocks. When the thermodynamic conditions change from laboratory conditions to typical conditions of the Italian storages, with the maximum reservoir pressure ranging from 150 to 180 bars and temperatures ranging from

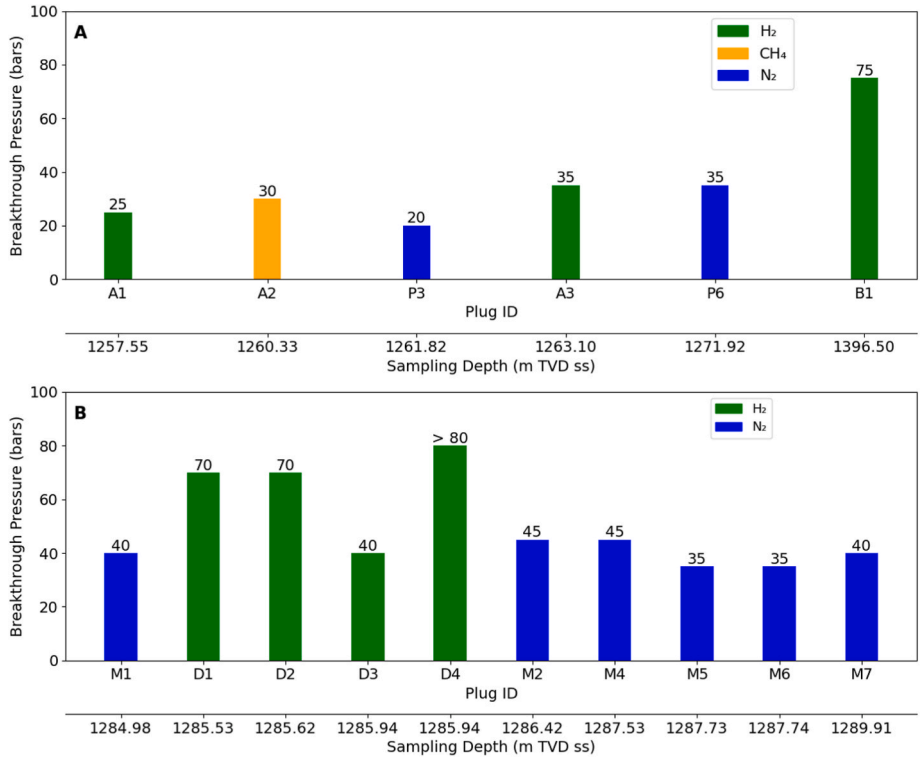

Fig. 10. Comparison of breakthrough pressure values obtained for hydrogen, methane and nitrogen on plugs from Caprock 1 (A) and on plugs from Caprock 2 (B).

45 °C to 50 °C, the pressure increase will adversely affect the capillary sealing capacity of the caprock, but the negative impact of the pressure increase might be partly offset by the temperature increase, especially in consideration of the caprock calcite content. Thus, even if a slight variation, likely a reduction, in the breakthrough pressure measured with laboratory experiments might occur under storage conditions, the caprock is expected to remain water-wet, as confirmed by experiments on clays under similar pressure and temperature conditions [52], and its sealing efficiency not compromised by hydrogen storage.

This work contributes to proving that the risk of hydrogen migration is not more enhanced than for nitrogen or methane for the clay-rich caprock Argille del Santerno, overlying most of the Italian depleted gas reservoirs under consideration for hydrogen storage; thus, underground hydrogen storage can be regarded as a feasible option to implement the energy transition.

Future work will be directed at investigating the impact of temperature on threshold pressure by testing additional caprock plugs under reservoir temperature conditions. Furthermore, it would be interesting to assess whether repeated reservoir pressure variation during storage cycles might affect the threshold pressure; however, the experimental procedure will have to be carefully conceived to achieve results truly representative of the real caprock behavior.

CRediT authorship contribution statement

Nacer Benlalam: Writing – review & editing, Writing – original draft, Visualization, Validation, Supervision, Methodology, Investigation, Formal analysis, Data curation, Conceptualization. **Nicolò Santi Vasile:** Writing – review & editing, Validation, Methodology, Investigation. **Costanzo Peter:** Writing – review & editing, Methodology, Investigation. **Vera Rocca:** Writing – review & editing, Methodology, Investigation, Conceptualization. **Dario Viberti:** Writing – review & editing, Validation, Formal analysis, Conceptualization. **Fabrizio Pirri:** Writing – review & editing, Resources, Project administration. **Vincenzo Pozzovivo:** Writing – review & editing, Validation, Data curation. **Andrea Mantegazzi:** Writing – review & editing. **Christian Coti:** Writing – review & editing. **Francesca Verga:** Writing – review & editing, Writing – original draft, Validation, Supervision, Project administration, Methodology, Funding acquisition, Formal analysis, Conceptualization.

Declaration of competing interest

The authors declare that they have no known competing financial interests or personal relationships that could have appeared to influence the work reported in this paper.

Acknowledgements

Nacer Benlalam's PhD scholarship is funded by the project National Recovery and Resilience Plan -NextGenerationEU, which has received funding from the Ministry of University and Research – Ministerial Decree 351/2022.

References

[1] Ball M, Weeda M. The hydrogen economy – Vision or reality?1. Int J Hydrogen Energy 2015;40:7903–19. https://doi.org/10.1016/j.ijhydene.2015.04.032.
[2] Miocic J, Heinemann N, Edlmann K, Scafidi J, Molaei F, Alcalde J. Underground hydrogen storage: a review, 528. Geological Society, London, Special Publications; 2023. p. 73–86. https://doi.org/10.1144/SP528-2022-88.
[3] Zivar D, Kumar S, Foroozesh J. Underground hydrogen storage: a comprehensive review. Int J Hydrogen Energy 2021;46:23436–62. https://doi.org/10.1016/j.ijhydene.2020.08.138.
[4] Kharel S, Shabani B. Hydrogen as a long-term large-scale energy storage solution to support renewables. Energies 2018;11:2825. https://doi.org/10.3390/en11102825.
[5] Hosseini M, Fahimpour J, Ali M, Keshavarz A, Iglauer S. Hydrogen wettability of carbonate formations: implications for hydrogen geo-storage. J Colloid Interface Sci 2022;614:256–66. https://doi.org/10.1016/j.jcis.2022.01.068.
[6] Benetatos C, Bocchini S, Carpignano A, Chiodoni A, Cocuzza M, Deangeli C, et al. How underground systems can contribute to meet the challenges of energy transition. Geoing Ambient Mineraria 2021. https://doi.org/10.19199/2021.163-164.1121-9041.065.
[7] Perera MSA. A review of underground hydrogen storage in depleted gas reservoirs: insights into various rock-fluid interaction mechanisms and their impact on the

process integrity. Fuel 2023;334:126677. https://doi.org/10.1016/j.fuel.2022.126677.
[8] Tarkowski R. Underground hydrogen storage: characteristics and prospects. Renew Sustain Energy Rev 2019;105:86–94. https://doi.org/10.1016/j.rser.2019.01.051.
[9] Al-Shafi M, Massarweh O, Abushaikha AS, Bicer Y. A review on underground gas storage systems: natural gas, hydrogen and carbon sequestration. Energy Rep 2023;9:6251–66. https://doi.org/10.1016/j.egyr.2023.05.236.
[10] Tawil M, Salina Borello E, Bocchini S, Pirri CF, Verga F, Coti C, et al. Solubility of H2-CH4 mixtures in brine at underground hydrogen storage thermodynamic conditions. Front Energy Res 2024;12. https://doi.org/10.3389/fenrg.2024.1356491.
[11] Tawil M, Borello ES, Panini F, Loffredo M, Bocchini S, Verga F, et al. PVT analysis for hydrogen and methane mixtures for underground hydrogen storage. OnePetro; 2024. https://doi.org/10.2118/220093-MS.
[12] Barison E, Donda F, Merson B, Le Gallo Y, Réveillère A. Citation: an insight into underground hydrogen storage in Italy. Nat Sustain 2023;2023:6886. https://doi.org/10.3390/su15086886.
[13] Bassani I, Bellini R, Vizzarro A, Coti C, Pozzovivo V, Barbieri D, et al. Biogeochemical characterization of four depleted gas reservoirs for conversion into underground hydrogen storage. Environ Microbiol 2023;25:3683–702. https://doi.org/10.1111/1462-2920.16538.
[14] Vasile N, Bellini R, Bassani I, Vizzarro A, Abdel Azim A, Coti C, et al. Innovative high pressure/high temperature, multi-sensing bioreactors system for microbial risk assessment in underground hydrogen storage. Int J Hydrogen Energy 2023;51. https://doi.org/10.1016/j.ijhydene.2023.10.245.
[15] Vasile NS, Suriano A, Bellini R, Bassani I, Vizzarro A, Coti C, et al. Biogeochemical modeling of high-pressure/high-temperature bioreactor systems for enhanced microbial risk assessment in underground hydrogen storage. SPE J 2025;30:1396–412. https://doi.org/10.2118/220064-PA.
[16] Bassani I, Bellini R, Vizzarro A, Vasile NS, Coti C, Pozzovivo V, et al. Systematic mapping of the potential microbiological risk associated with underground hydrogen storage in depleted gas reservoirs on the Italian territory. OnePetro 2025. https://doi.org/10.2118/225567-MS.
[17] Bellini R, Vasile NS, Bassani I, Vizzarro A, Coti C, Barbieri D, et al. Investigating the activity of indigenous microbial communities from Italian depleted gas reservoirs and their possible impact on underground hydrogen storage. Front Microbiol 2024;15. https://doi.org/10.3389/fmicb.2024.1392410.
[18] Panini F, Ghanbarian B, Salina Borello E, Viberti D. Estimating geometric tortuosity of saturated rocks from micro-CT images using percolation theory. Transport Porous Media 2024;151:1–28. https://doi.org/10.1007/s11242-024-02085-w.
[19] Viberti D, Peter C, Salina Borello E, Panini F. Pore structure characterization through path-finding and lattice boltzmann simulation. Adv Water Resour 2020;141:103609. https://doi.org/10.1016/j.advwatres.2020.103609.
[20] Verga F. What's conventional and what's special in a reservoir study for underground GasStorage. Energies 2018;11(5):1245. https://doi.org/10.3390/en11051245.
[21] Salina Borello E, Bocchini S, Chiodoni A, Coti C, Fontana M, Panini F, et al. Underground hydrogen storage safety: experimental study of hydrogen diffusion through caprocks. Energies 2024;17:394. https://doi.org/10.3390/en17020394.
[22] Vinsot A, Appelo CAJ, Lundy M, Wechner S, Lettry Y, Lerouge C, et al. In situ diffusion test of hydrogen gas in the opalinus clay, 400. Geological Society, London, Special Publications; 2014. p. 563–78. https://doi.org/10.1144/SP400.12.
[23] Krooss BM, Leythaeuser D, Schaefer RG. The quantification of diffusive hydrocarbon losses through cap rocks of natural gas reservoirs—A Reevaluation1. AAPG Bull 1992;76:403–6. https://doi.org/10.1306/BDFF881C-1718-11D7-8645000102C1865D.
[24] Reitenbach V, Ganzer L, Albrecht D, Hagemann B. Influence of added hydrogen on underground gas storage: a review of key issues. Environ Earth Sci 2015;73. https://doi.org/10.1007/s12665-015-4176-2.
[25] Shi Z, Jessen K, Tsotsis TT. Impacts of the subsurface storage of natural gas and hydrogen mixtures. Int J Hydrogen Energy 2020;45:8757–73. https://doi.org/10.1016/j.ijhydene.2020.01.044.
[26] Ibrahim MA, Tek MR, Katz DL. Threshold pressure in gas storage. Washington, DC, USA: American Gas Association; 1971.
[27] Li S, Dong M, Li Z, Huang S, Qing H, Nickel E. Gas breakthrough pressure for hydrocarbon reservoir seal rocks: implications for the security of long-term CO2 storage in the weyburn field. Geofluids 2005;5:326–34. https://doi.org/10.1111/j.1468-8123.2005.00125.x.
[28] Wu T, Pan Z, Connell LD, Liu B, Fu X, Xue Z. Gas breakthrough pressure of tight rocks: a review of experimental methods and data. J Nat Gas Sci Eng 2020;81:103408. https://doi.org/10.1016/j.jngse.2020.103408.
[29] Egermann P, Lenormand R. Measurement of capillary pressure curves at reservoir conditions. 2002.
[30] Hildenbrand A, Schlömer S, Krooss BM, Littke R. Gas breakthrough experiments on pelitic rocks: comparative study with N2, CO2 and CH4. Geofluids 2004;4:61–80. https://doi.org/10.1111/j.1468-8123.2004.00073.x.
[31] Ito D, Akaku K, Okabe T, Takahashi T, Tsuji T. Measurement of threshold capillary pressure for seal rocks using the step-by-step approach and the residual pressure approach. Energy Proc 2011;4:5211–8. https://doi.org/10.1016/j.egypro.2011.02.499.
[32] Amann A, Waschbüsch M, Bertier P, Busch A, Krooss BM, Littke R. Sealing rock characteristics under the influence of CO2. Energy Proc 2011;4:5170–7. https://doi.org/10.1016/j.egypro.2011.02.494.
[33] Li Q, Gates ID, Hejazi SH. Experimental investigation of caprock sealing capacity for underground hydrogen storage. Int J Hydrogen Energy 2025;165:150858. https://doi.org/10.1016/j.ijhydene.2025.150858.
[34] Thomas LK, Katz DL, Tek MR. Threshold pressure phenomena in porous media. Soc Petrol Eng J 1968;8:174–84. https://doi.org/10.2118/1816-PA.
[35] Ali M, Jha NK, Al-Yaseri A, Zhang Y, Iglauer S, Sarmadivaleh M. Hydrogen wettability of quartz substrates exposed to organic acids; implications for hydrogen geo-storage in sandstone reservoirs. J Petrol Sci Eng 2021;207:109081. https://doi.org/10.1016/j.petrol.2021.109081.
[36] Al-Mukainah H, Al-Yaseri A, Yekeen N, Hamad JA, Mahmoud M. Wettability of shale–brine–H2 system and H2-brine interfacial tension for assessment of the sealing capacities of shale formations during underground hydrogen storage. Energy Rep 2022;8:8830–43. https://doi.org/10.1016/j.egyr.2022.07.004.
[37] Al-Yaseri A, Yekeen N, Mahmoud M, Kakati A, Xie Q, Giwelli A. Thermodynamic characterization of H2-brine-shale wettability: implications for hydrogen storage at subsurface. Int J Hydrogen Energy 2022;47:22510–21. https://doi.org/10.1016/j.ijhydene.2022.05.086.
[38] Hosseini M, Fahimpour J, Ali M, Keshavarz A, Iglauer S. H2−brine interfacial tension as a function of salinity, temperature, and pressure; implications for hydrogen geo-storage. J Petrol Sci Eng 2022;213:110441. https://doi.org/10.1016/j.petrol.2022.110441.
[39] Hosseini M, Ali M, Fahimpour J, Keshavarz A, Iglauer S. Basalt-H2-brine wettability at geo-storage conditions: implication for hydrogen storage in basaltic formations. J Energy Storage 2022;52:104745. https://doi.org/10.1016/j.est.2022.104745.
[40] Aghaei H, Al-Yaseri A, Toorajipour A, Shahsavani B, Yekeen N, Edlmann K. Host-rock and caprock wettability during hydrogen drainage: implications of hydrogen subsurface storage. Fuel 2023;351:129048. https://doi.org/10.1016/j.fuel.2023.129048.
[41] Janjua AN, Ali M, Murtaza M, Patil S, Kamal MS. Effects of salinity, temperature, and pressure on H2–brine interfacial tension: implications for underground hydrogen storage. J Energy Storage 2024;95:112510. https://doi.org/10.1016/j.est.2024.112510.
[42] Alessa S, Sakhaee-Pour A. Hydrogen unclogging of caprock. Int J Hydrogen Energy 2024;77:434–40. https://doi.org/10.1016/j.ijhydene.2024.06.234.
[43] Ghaedi M, Østebø Andersen P, Gholami R. Maximum column height and optimum storage depth for geological storage of hydrogen. Int J Hydrogen Energy 2024;50:291–304. https://doi.org/10.1016/j.ijhydene.2023.07.071.
[44] Eid C, Benetatos C, Rocca V. Fluid production dataset for the assessment of the anthropogenic subsidence in the Po plain area (Northern Italy). Resources 2022;11:53. https://doi.org/10.3390/resources11060053.
[45] Tek MR. Underground storage of natural gas. Houston: Gulf Pub. Co. Book Division; 1987.
[46] Blunt MJ. Multiphase flow in permeable media: a pore-scale perspective. Cambridge: Cambridge University Press; 2017. https://doi.org/10.1017/9781316145098.
[47] Hildenbrand A, Schlömer S, Krooss BM. Gas breakthrough experiments on fine-grained sedimentary rocks. Geofluids 2002;2:3–23. https://doi.org/10.1046/j.1468-8123.2002.00031.x.
[48] Minardi A, Stavropoulou E, Kim T, Ferrari A, Laloui L. Experimental assessment of the hydro-mechanical behaviour of a shale caprock during CO2 injection. Int J Greenh Gas Control 2021;106. https://doi.org/10.1016/j.ijggc.2020.103225.
[49] Heath JE, Dewers TA, McPherson BJOL, Nemer MB, Kotula PG. Pore-lining phases and capillary breakthrough pressure of mudstone caprocks: sealing efficiency of geologic CO2 storage sites. Int J Greenh Gas Control 2012;11:204–20. https://doi.org/10.1016/j.ijggc.2012.08.001.
[50] Slowinski EJJr, Gates EE, Waring CE. The effect of pressure on the surface tensions of liquids. J Phys Chem 1957;61:808–10. https://doi.org/10.1021/j150552a028.
[51] Massoudi R, King ADJr. Effect of pressure on the surface tension of water. Adsorption of low molecular weight gases on water at 25.deg. J Phys Chem 1974;78:2262–6. https://doi.org/10.1021/j100615a017.
[52] Al-Yaseri A, Wolff-Boenisch D, Fauziah CA, Iglauer S. Hydrogen wettability of clays: implications for underground hydrogen storage. Int J Hydrogen Energy 2021;46:34356–61. https://doi.org/10.1016/j.ijhydene.2021.07.226.
[53] Zhang C, Wang M. A critical review of breakthrough pressure for tight rocks and relevant factors. J Nat Gas Sci Eng 2022;100:104456. https://doi.org/10.1016/j.jngse.2022.104456.
[54] Gbadamosi AO, Muhammed NS, Patil S, Al Shehri D, Haq B, Epelle EI, et al. Underground hydrogen storage: a critical assessment of fluid-fluid and fluid-rock interactions. J Energy Storage 2023;72:108473. https://doi.org/10.1016/j.est.2023.108473.
[55] van Rooijen WA, Habibi P, Xu K, Dey P, Vlugt TJH, Hajibeygi H, et al. Interfacial tensions, solubilities, and transport properties of the H2/H2O/NaCl system: a molecular simulation study. J Chem Eng Data 2024;69:307–19. https://doi.org/10.1021/acs.jced.2c00707.
[56] Yekeen N, Al-Yaseri A, Negash BM, Ali M, Giwelli A, Esteban L, et al. Clay-hydrogen and clay-cushion gas interfacial tensions: implications for hydrogen storage. Int J Hydrogen Energy 2022;47:19155–67. https://doi.org/10.1016/j.ijhydene.2022.04.103.
[57] Esfandyari H, Sarmadivaleh M, Esmaeilzadeh F, Ali M, Iglauer S, Keshavarz A. Experimental evaluation of rock mineralogy on hydrogen-wettability: implications for hydrogen geo-storage. J Energy Storage 2022;52:104866. https://doi.org/10.1016/j.est.2022.104866.
[58] Janjua AN, Ali M, Kamal MS, Patil S, Hoteit H, Raza A, et al. Experimental insights into surface wettability alterations and solvent adsorption effects on porous sandstone and carbonate rocks in H_2-brine systems: implications for underground

hydrogen storage. J Energy Storage 2025;139:118808. https://doi.org/10.1016/j.est.2025.118808.
[59] Schowalter TT. Mechanics of secondary hydrocarbon migration and Entrapment1. AAPG Bull 1979;63:723–60. https://doi.org/10.1306/2F9182CA-16CE-11D7-8645000102C1865D.
[60] Egermann P, Lombard J-M, Bretonnier P. A fast and accurate method to measure threshold capillary pressure of caprocks under representative conditions. 2006.
[61] Schlömer S, Krooss BM. Experimental characterisation of the hydrocarbon sealing efficiency of cap rocks. Mar Petrol Geol 1997;14:565–80. https://doi.org/10.1016/S0264-8172(97)00022-6.
[62] Vassenden F, Sylta Ø, Zwach C. Secondary migration in a 2D visual laboratory model. 2003. https://doi.org/10.3997/2214-4609.201405814.
[63] Zweigel P, Lindeberg E, Moen A, Wessel-Berg D. Towards a methodology for top seal efficacy assessment for underground CO2 storage. In: Rubin ES, Keith DW, Gilboy CF, Wilson M, Morris T, Gale J, et al., editors. Greenhouse gas control technologies 7. Oxford: Elsevier Science Ltd; 2005. p. 1323–8. https://doi.org/10.1016/B978-008044704-9/50145-2.
[64] Benetatos C, Rocca V, Verga F, Adinolfi L, Marzano F. Deformation behavior of a regional shale formation from integrated laboratory and well data analysis: insights for underground fluid storage in northern Italy. Geoenergy Sci Eng 2023;229:212109. https://doi.org/10.1016/j.geoen.2023.212109.
[65] ASTM D2487-10. Standard practice for classification of soils for engineering purposes. Unified Soil Classification System); 2010. https://doi.org/10.1520/D2487-10.
[66] ASTM D6913-04. Standard test methods for particle-size distribution (Gradation) of soils using sieve analysis. https://doi.org/10.1520/D6913-04; 2004.
[67] ASTM D7928-17. Standard test method for particle-size distribution (Gradation) of fine-grained soils using the sedimentation (Hydrometer) analysis. https://doi.org/10.1520/D7928-17; 2017.
[68] Ingram RL. Fissility of mudrocks. Geol Soc Am Bull 1953;64:869–78. https://doi.org/10.1130/0016-7606(1953)64%5B869:FOM%5D2.0.CO;2.
[69] Rietveld HM. A profile refinement method for nuclear and magnetic structures. J Appl Cryst 1969;2:65–71. https://doi.org/10.1107/S0021889869006558.
[70] Chiodoni A, Fontana M, Bejtka K, Gho CI, Marzano F, Pozzovivo V, et al. Reservoir and caprock compositional assessment strategy for hydrogen storage. OnePetro 2024. https://doi.org/10.2118/220077-MS.
[71] Rocca V. The sealing efficiency of cap rocks – laboratory tests and an empirical correlation - geam journal. GEAM 2021. https://doi.org/10.19199/2021.162.1121-9041.041.
[72] Busch A, Amann-Hildenbrand A. Predicting capillarity of mudrocks. Mar Petrol Geol 2013;45:208–23. https://doi.org/10.1016/j.marpetgeo.2013.05.005.
[73] Li Y, Zhao J, Zhao S, Li Q, Li X, Yu Q. Numerical simulation analysis of CH4 breakthrough pressure in partially saturated low-permeability rock sample under multiple P-T conditions. J Hydrol 2023;626:130331. https://doi.org/10.1016/j.jhydrol.2023.130331.
[74] Zhao Y, Yu Q. Effect of CH4 on the CO2 breakthrough pressure and permeability of partially saturated low-permeability sandstone in the Ordos Basin, China. J Hydrol 2018;556:732–48. https://doi.org/10.1016/j.jhydrol.2017.11.030.
[75] Sun J, Dong Z, Zhu S, Tian S, Zhou J. Pore structure evolution of mudstone caprock under cyclic load-unload and its influence on breakthrough pressure. Front Earth Sci 2023;17:691–700. https://doi.org/10.1007/s11707-022-1019-9.
[76] Mi L, Guo Y, Li Y, Zeng D, Lu C, Zhang G. Evaluation of the dynamic sealing performance of cap rocks of underground gas storage under multi-cycle alternating loads. Energy Geosci 2024;5:100319. https://doi.org/10.1016/j.engeos.2024.100319.
[77] Ajibona A, Pandey R, Khanal A, Zenali SM, Abdelaziz SL. Pycnometric evaluation of shale caprocks during underground hydrogen storage in depleted reservoirs. Int J Hydrogen Energy 2025;101:1312–28. https://doi.org/10.1016/j.ijhydene.2024.12.427.
[78] Zhou X, Lü X, Sui F, Wang X, Li Y. The breakthrough pressure and sealing property of lower Paleozoic carbonate rocks in the Gucheng area of the Tarim Basin. J Petrol Sci Eng 2022;208:109289. https://doi.org/10.1016/j.petrol.2021.109289.
[79] Esfandyari H, Hosseini M, Ali M, Iglauer S, Haghighi M, Keshavarz A. Assessment of the interfacial properties of various mineral/hydrogen/water systems. J Energy Storage 2023;60:106637. https://doi.org/10.1016/j.est.2023.106637.
[80] Hosseini M, Ali M, Fahimpour J, Keshavarz A, Iglauer S. Calcite–fluid interfacial tension: H2 and CO2 geological storage in carbonates. Energy Fuel 2023;37:5986–94. https://doi.org/10.1021/acs.energyfuels.3c00399.
[81] Pan B, Yin X, Iglauer S. Rock-fluid interfacial tension at subsurface conditions: implications for H2, CO2 and natural gas geo-storage. Int J Hydrogen Energy 2021;46:25578–85. https://doi.org/10.1016/j.ijhydene.2021.05.067.
[82] Hosseini M, Ali M, Fahimpour J, Keshavarz A, Iglauer S. Assessment of rock-hydrogen and rock-water interfacial tension in shale, evaporite and basaltic rocks. J Nat Gas Sci Eng 2022;106:104743. https://doi.org/10.1016/j.jngse.2022.104743.
[83] Hosseini M, Fahimpour J, Ali M, Keshavarz A, Iglauer S. Capillary sealing efficiency analysis of caprocks: implication for hydrogen geological storage. Energy Fuel 2022;36:4065–75. https://doi.org/10.1021/acs.energyfuels.2c00281.
[84] Omrani S, Ghasemi M, Singh M, Mahmoodpour S, Zhou T, Babaei M, et al. Interfacial tension–temperature–pressure–salinity relationship for the hydrogen–brine system under reservoir conditions: integration of molecular dynamics and machine learning. Langmuir 2023;39:12680–91. https://doi.org/10.1021/acs.langmuir.3c01424.
[85] Ajibona A, Pandey R. Strain-based assessment of shale caprock during cyclic underground hydrogen storage. Energy Fuel 2025;39:11053–66. https://doi.org/10.1021/acs.energyfuels.5c00783.
[86] Yan W, Zhao G-Y, Chen G-J, Guo T-M. Interfacial tension of (Methane + Nitrogen) + water and (Carbon Dioxide + Nitrogen) + water systems. J Chem Eng Data 2001;46:1544–8. https://doi.org/10.1021/je0101505.
[87] Ren Q-Y, Chen G-J, Yan W, Guo T-M. Interfacial tension of (CO_2 + CH_4) + water from 298 K to 373 K and pressures up to 30 MPa. J Chem Eng Data 2000;45(4):610–2. https://doi.org/10.1021/je990301s.
[88] Iglauer S, Ali M, Keshavarz A. Hydrogen wettability of sandstone reservoirs: implications for hydrogen Geo-Storage. Geophys Res Lett 2021. https://doi.org/10.1029/2020GL090814.